2
3 **Review article: Performance assessment of electromagnetic wave-based**
4 **field sensors for SWE monitoring**
5

7 Alain Royer[a,b*], Alexandre Roy[c,b], Sylvain Jutras[d], Alexandre Langlois[a,b]
8
9 [a]Centre d'Applications et de Recherche en Télédétection (CARTEL), Université de Sherbrooke, Sherbrooke,
10 Québec, Canada
11 [b]Centre d'études nordiques, Québec, Canada
12 [c]Département des Sciences de l'Environnement, Université du Québec à Trois-Rivières, Trois-Rivières,
13 Québec, Canada
14 [d]Département des sciences du bois et de la forêt, Université Laval, Québec City, Québec, Canada
15 * Corresponding author

17 **Abstract** (138 words)
18 Continuous and spatially distributed data of snow mass (snow water equivalent, SWE)
19 from automatic ground-based measurements are increasingly required for climate
20 change studies and for hydrological applications (snow hydrological model improvement
21 and data assimilation). We present and compare four new-generation non-invasive
22 sensors that are based on electromagnetic waves for direct measurements of SWE:
23 Cosmic Ray Neutron Probe (CNRP); Gamma Ray Monitoring (GMON) scintillator;
24 frequency-modulated continuous-wave radar (FMCW-Radar) at 24 GHz; and Global
25 Navigation Satellite System (GNSS). All four techniques are relatively low cost, have low
26 power requirements, provide continuous and autonomous measurements, and can be
27 installed in remote areas. Their operating principles are briefly summarized before
28 examples of comparative measurements are provided. A performance review comparing
29 their advantages, drawbacks and accuracies is discussed. Overall instrument accuracy is
30 estimated to range between 9 and 15%.
31
32 **Key word:** Snow Water Equivalent, electromagnetic wave sensors, Cosmic Ray Neutron
33 Probe, Gamma Ray Monitoring, frequency-modulated continuous-wave radar, Global
34 Navigation Satellite System, sensor performance review

35

36 **1. Introduction**
37 Snow cover on the ground plays an important role in the climate system due to its high
38 albedo, heat insulation that affects the ground thermal regime, and its contribution to
39 snow runoff and soil moisture. The snow water equivalent (SWE, its mass per unit area,
40 kg m^{-2}, or in mm) is an Essential Climate Variable (ECV) for monitoring climate change, as
41 recognized by the Global Climate Observing System (GCOS, WMO-UN_E), in line with the
42 WMO-Global Cryosphere Watch Initiative (Key et al., 2015;
43 https://globalcryospherewatch.org). SWE monitoring is also of primary importance for
44 hydrological forecasting and to prevent flooding risks over snowmelt-dominated basins

45   in mountainous and cold climate regions. The distribution of snow stations is generally
46   sparse in high latitude regions, remote areas and high mountains (Bormann et al., 2013;
47   Global Cryosphere Watch, 2015; Key et al., 2015; Pirazzini et al., 2018; Brown et al., 2019,
48   2021; Royer et al., 2021), given that monitoring is generally based upon expensive and
49   occasional (weekly to monthly) manual sampling. The automation of manual survey
50   networks is an essential medium-term prospect, especially since reliable and automatic
51   instrument alternatives exist (Dong, 2018; Brown et al., 2021).
52
53   Various in situ field devices and approaches for measuring the temporal dynamics of SWE
54   are available, all of which have their strengths and limitations (see the review by
55   Rasmussen et al., 2012; Kinar and Pomeroy, 2015; Pirazzini et al., 2018). Some are invasive
56   (i.e., destroying the snowpack or changing its properties), while others that are based on
57   different remotely sensed approaches are non-invasive. Here, we focus on a new
58   generation of electromagnetic wave-based field sensors that directly measure SWE, i.e.,
59   measuring a signal that is proportional to the snow mass per unit area. In this study, we
60   do not consider indirect approaches, such as those that are based on snow depth
61   monitoring, combined with snow density model evolution (Yao et al., 2018). We also do
62   not consider satellite-based approaches.
63
64   The objective of this paper, therefore, is to present a performance review of four selected
65   non-invasive sensors (Table 1), viz., the Cosmic Ray Neutron Probe (CNRP), the Gamma
66   Ray Monitoring (GMON) scintillator, frequency-modulated continuous-wave radar
67   (FMCW-Radar) and Global Navigation Satellite System (GNSS) receivers. All four
68   approaches have common features: relatively low cost; low power; providing continuous
69   and autonomous SWE measurements; and deployable in remote areas. Surface-based
70   radar scatterometers and microwave radiometers have not been considered in this study
71   because 1) they are still in early stages of development or are currently not operational,
72   and 2) they have heavy maintenance demands (not autonomous) and are relatively
73   expensive. These include, for example, scatterometers (Werner et al., 2010; Wiesmann
74   et al., 2010; King et al., 2015; Werner et al., 2019), microwave radiometers (Langlois,
75   2015; Roy et al., 2016, 2017; Wiesmann et al., 2021); radar interferometers (Werner et
76   al., 2010; Leinss et al., 2015; Pieraccini and Miccinesi, 2019; GPRI brochure, 2021), and
77   Stepped-Frequency Continuous Wave Radar (SFCW) instruments (Alonso et al., 2021).
78
79   Sect. 2 provides background information on the basic principles of each of the four
80   sensors that are presented in Table 1. Examples of SWE temporal series comparisons from
81   the four different instruments are given in Sect. 3, permitting an evaluation of the
82   performance of each system, including accuracy analysis. Advantages and drawbacks of
83   these sensors are then discussed in Sect. 4.
84
85   **2.** Electromagnetic wave-based SWE sensor review
86   The main characteristics of the four reviewed sensors are summarized in Table 1, with the
87   acronym that is used to denote them, together with their commercial names. There are
88   two operation modes for the Cosmic Ray Neutron Probe (CNRP); thus, five cases were

89 considered. All of these sensors allow quasi-continuous measurements throughout the
90 winter without maintenance, and are powered by solar panels and batteries. The
91 measuring principles of each of the instruments are illustrated in Fig. 1 and shown in Fig.
92 2. In this section, we only recall the main principle of functioning and the key elements of
93 SWE retrieval, given that all sensors are well described in detail in the cited references.
94
95 *Table 1. SWE sensors that were studied and acronyms that were used. FMCW: frequency-*
96 *modulated continuous-wave radar; GNSS: Global Navigation Satellite System, including*
97 *GPS (USA), GLONASS (Russia), Galileo (Europe) and Beidou (China) satellite constellations.*
98 *The frequency (Freq.) of the electromagnetic wave that was used and their approximate*
99 *maximum Snow Water Equivalent (SWE$_{max}$) measurement limit capabilities are given. See*
100 *Fig. 1 for experimental settings and Fig. 2 for photos.*
101

Sensor	Acronym	Approach	Freq. GHz	SWE$_{max}$ (mm)	Comments	Commercial Name	Main recent references
Cosmic Ray Neutron Probe	CRNP	Sensor beneath snowpack	10^{23}	>2000	Measures total snow, ice and water amount	SnowFox NRC EDF-Fr	https://hydroinnova.com Gottardi et al., 2013
		Sensor above snowpack		~ 150-300		Hydroinnova CRS-1000/B	https://hydroinnova.com Bogena et al., 2020
Gamma Ray scintillator	GMON	Sensor above snowpack	3.53 10^{11} 6.31 10^{11}	~ 800	Measures total snow, ice and water amount	CS725 Campbell Sci.	Choquette et al., 2013 Smith et al., 2017 http://www.campbellsci.ca
Frequency-modulated continuous-wave Radar	FMCW-Radar	Active sensor above snowpack	24	~1000	Requires snow depth measurements Also measures stratigraphy	Sentire™ sR-1200 IMST Inc.	Pomerleau et al., 2020 https://shop.imst.de
Global Navigation Satellite System receivers	GNSSR	2 antennas above/ beneath snowpack	1.575 - 1.609	>1500	Measures also Snow depth and Liquid Water Content	SnowSense	Henkel et al., 2019 Koch et al., 2020 https://www.vista-geo.de/en/snowsense/

102
103
104
105
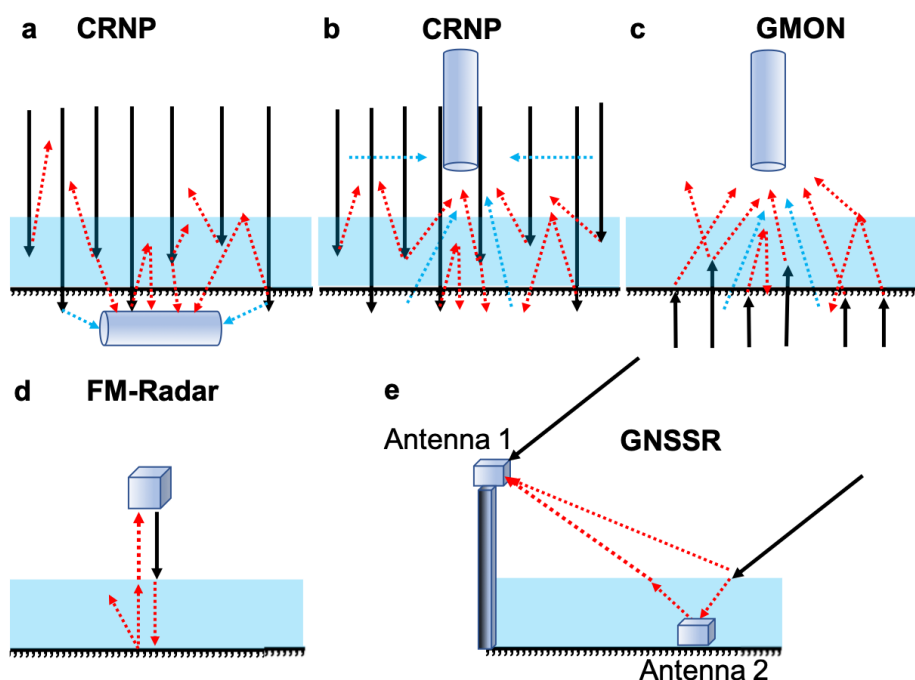
106
107 Figure 1 Diagram of electromagnetic ray paths for the four SWE sensors (see Table 1). In all figures, black
108 arrows correspond to natural or emitted electromagnetic signals and dotted red arrows to rays interacting
109 with snow (the lower the signal reaching the sensor, the higher the SWE). **a)** Cosmic Ray Neutron Probe
110 (CNRP) below the snow, buried in the ground. In this case, black arrows are ambient neutrons generated
111 primarily by interactions of secondary cosmic ray neutrons with terrestrial and atmospheric nuclei. Dotted
112 red arrows are neutrons interacting with snow, which decrease when SWE increases. Dotted blue arrows
113 are neutrons interacting with soil moisture. **b)** CNRP above the snow, looking downward. Same as (a) for
114 the arrow meanings, but dotted blue arrows are neutrons interacting with soil and atmospheric moisture.
115 **c)** Gamma Monitor (GMON) sensor. Same as (a) for the arrow meanings. **d)** Frequency-modulated
116 continuous-wave radar (FMCW-Radar) looking downward above the snow. Black arrow is the radar-emitted
117 wave at 24 GHz. **e)** Global Navigation Satellite System (GNSS) Receivers. The two antennas receive signals
118 emitted by all of the GNSS satellites in the antennas' field of view and at all incidence angles (only one ray
119 at one angle is shown).
120

121
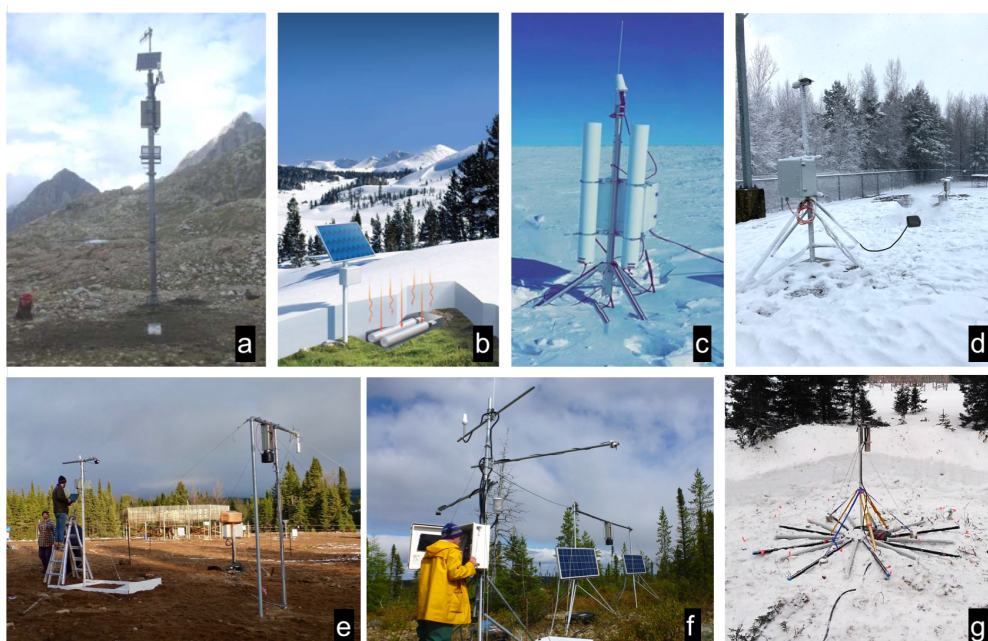
Figure 2. Photographs of sensors that were analyzed. **a)** Cosmic Ray Neutron Probe (CNRP) from the EDF
French network (Nivomètre à Rayon Cosmic, NRC) at Spijeoles, French Pyrénées. One can see the neutron
probe buried in the ground (sensor composed of two neutron detector tubes filled with Helium 3 (^{3}He) and
placed at 3.5 m from a 6 m mast, which carries the ancillary sensors (atmospheric pressure, temperature,
snow height, wind, liquid precipitation). Credit: Gottardi et al. (2013). **b)** SnowFox CNRP set at ground level
beneath the snow cover. The system is composed of two detector tubes filled with $^{10}BF_3$; one is sensitive to
neutrons with a maximum energy of ~0.025 eV, whereas the second is sensitive to moderated energy
neutrons from ~0.2eV to 100 keV. Similar to (a), the system requires measurements of atmospheric
conditions (atmospheric pressure, temperature and humidity). Credit: Hydroinnova SnowFox manual. **c)**
Same sensor as in (b), but the Hydroinnova CRS-1000/B sensor is placed above the snow, measuring the
ambient and upward neutron counts, with the latter being attenuated by the snowpack. Crédit: Philip
Marsh, Wilfrid Laurier University, Waterloo, ON, Canada; sensor in the tundra at Trail Valley Creek, Changing
Cold Regions Network http://ccrnetwork.ca). **d)** GNSSR installed at the Université de Sherbrooke SIRENE
site. The antenna that was placed on the ground (beneath the snow) was made visible at 3 m from the mast,
on top of which a second antenna was affixed. Credits: Alain Royer. **e)** The FMCW-Radar (on the left) and
the GMON (on the right) at the NEIGE-Forêt Montmorency site. The housing of the IMST sentire™ FMCW-
Radar module is compact (114.0 mm × 87.0 mm × 42.5 mm) and weighs 280 g. A metallic plate on the
ground in the field-of-view of the radar substantially increases radar echoes. The GMON is a tube 62 cm
long, and 13 cm in diameter, weighing 9 kg. In the background of photo **e**, one can see the solid precipitation
gauge, which is known as the Double Fence Intercomparison Reference (DFIR). Credits: Alain Royer. **f)**
Meteorological and snow (GMON) automatic station at the LeMoyne James-Bay, Québec, Canada site in a
sub-arctic environment (Prince et al., 2019). Credits: Alain Royer. **g)** The GMON at the NEIGE-Forêt
Montmorency site set up to boost ^{40}K counts with pipes filled with potassium fertilizer. Credit: Sylvain
Jutras.

2.1 Cosmic Ray Neutron probe (CRNP)

CRNP measurement is based on the moderation of ambient neutrons by hydrogen in
water, snow and ice. The intensity of natural low-energy cosmic ray neutron emission is

149 inversely correlated with the amount of hydrogen in the soil (Zreda et al. 2008; Andreasen
150 et al., 2017) or snow cover (Desilets et al. 2010; Gottardi et al., 2013; Sigouin and Si, 2016;
151 Bogena et al., 2020). Even though the principle of this approach has been known since
152 the 1970s, it attained a level of operational maturity in the 2000s, especially with the use
153 of commercialized soil moisture probes. Électricité de France (EDF) successfully used a
154 network of cosmic-ray probes (detector based on a Helium counter) that were buried
155 under the snowpack to measure SWE for more than a decade in the French Alps and in
156 the Pyrenees (Fig. 2a) (Paquet and Laval, 2006; Paquet et al., 2008; Gottardi et al., 2013).

157
158 There are two experimental approaches for CNRP-based SWE monitoring (Fig. 1a,b), i.e.,
159 1) with the probe at the ground level beneath the snow (Figs. 1a, 2b, such as the SnowFox
160 sensor), or 2) with the probe placed a few meters above the snow surface (Fig. 1b), such
161 as the one proposed by Hydroinnova (Fig. 2c) (CRS-1000/B, Hydroinnova, Albuquerque,
162 NM, USA; http://hydroinnova.com/snow_water.html). Using a dual-channel (fast and
163 slow neutrons) cosmic ray probe above the snowpack (Fig. 1b) is an attractive SWE
164 measurement tool because it can provide direct estimates of SWE within a 20 to 40 ha
165 footprint (20 ha corresponds to a circle of 252 m radius) (Desilets and Zerda, 2013;
166 Schattan et al., 2017). In contrast, the footprint of a probe that is installed under the snow
167 is limited to a spot measurement above the sensor (Fig. 1a). While approach (1a) permits
168 measurements of very thick snow cover (> 1000 mm SWE), the drawback of approach (1b)
169 is that it is limited to low SWE measurements (typically < 150 mm SWE) over
170 homogeneous flat terrain. However, In the Austrian Alps, contrary to previous studies,
171 Schattan et al. claim not to have measured saturation for a snowpack of the order of 600
172 mm SWE, over an estimated footprint with 230 m radius. Aspects that are related to the
173 measurement scale of each sensor are critical to SWE measurements, since SWE is
174 generally highly variable spatially, depending upon the ecosystem and terrain (Kinar and
175 Pomeroy, 2015; Dong, 2018). These questions are discussed in Sect. 4.

176
177 The CRNP method requires creating a function for converting neutron counts to snow
178 water equivalent (Paquet et al., 2008; Gottardi et al., 2013; Sigouin and Si, 2016;
179 Andreasen et al., 2017; Schattan et al., 2017; Bogena et al., 2020). Desilets (2017) provides
180 the calibration procedure in detail. Neutron counts must be accumulated over a specified
181 period of time (e.g., from 6 h to 24 h). The CRNP method requires that the counting rate
182 must first be known (calibrated) and that disturbance effects on measured cosmic rays at
183 the site location have to be taken into account. Disturbance effects that need to be
184 corrected include temporal variations in the natural cosmic-ray flux and variations in air
185 pressure and atmospheric water vapor on site measurements during the count time.
186 Temporal variation in cosmic-ray flux can be determined from the NMDB database (Real-
187 Time Database for high-resolution Neutron Monitor measurements; www.nmdb.eu),
188 thereby providing access to reference neutron monitor measurements from stations
189 around the world. Corrections for air pressure (linked to the altitude of the station) and
190 atmospheric water vapor variations require ancillary standard meteorological sensors,
191 which measure atmospheric pressure, air temperature and relative humidity.
192

193 While accuracy losses that are linked to atmospheric disturbances (pressure and humidity
194 corrections) are relatively weak (a few percent), this is not the case for primary variations
195 in the natural cosmic-ray flux (Andreasen et al., 2017), which may drastically change the
196 results of SWE estimation. This flux can vary up to 30% over long periods (weeks to
197 months), thereby causing errors up to 50% in SWE estimates when they are not
198 considered (Paquet and Laval, 2006). Therefore, it is important to correct the measured
199 signal using the closest world reference station in the vicinity of the measurement site. If
200 not available, a second cosmic-ray sensor is required to produce accurate SWE estimates
201 using normalized signals (above and beneath snow).
202
203 In the case of the second approach, where the probe is installed above the ground surface
204 (Fig. 1b), the probe must be calibrated for soil moisture. If soil moisture correction is not
205 applied on the winter signal measurements, retrieved SWE values will be systematically
206 overestimated. This bias can be corrected using measurements of CRNP signal without
207 snow, just prior to ~~snowfall~~. We must either assume that soil moisture levels remain
208 stable throughout the winter, which is generally the case when soil remains frozen, or
209 apply a correction based on soil moisture conditions that are otherwise known.
210
211 2.2 Gamma Ray scintillator (GMON)
212 Monitoring snow water equivalent by using natural soil radioactivity is a well-known
213 approach (Bissell and Peck, 1973). Since 1980, an airborne snow survey program using
214 this technology has successfully collected areal mean SWE data for operational flood
215 forecasting over the whole northwestern North America, including Rocky Mountains,
216 Alaska and Great Plains (National Operational Hydrologic Remote Sensing Center,
217 https://www.nohrsc.noaa.gov/snowsurvey/). The mean areal SWE value is based on the
218 difference between gamma radiation measurements over bare ground and snow-covered
219 ground, the latter being attenuated by the snowpack (Carroll, 2001).
220
221 The principle of SWE measurements that are based on the Gamma Monitor (GMON) ray
222 scintillator is the absorption by the water, regardless of its phase (liquid, snow or ice), of
223 the natural radioactive emission of Potassium-40 (^{40}K) from soils (Ducharme et al., 2015).
224 This naturally occurring radioactive isotope of potassium has a gamma emission of 1.46
225 MeV. The GMON probe that is manufactured by Campbell Scientific (Canada) (CS7525;
226 http://www.campbellsci.ca/cs725) also measures the emission of Thallium-208 (^{208}Tl),
227 which emits gamma rays at a slightly higher energy (2.61 MeV) that originate from the
228 decay of Thorium 232 (Choquette et al., 2013; Wright, 2013; Stranden et al., 2015). Both
229 of these elements are common to almost all types of surfaces, regardless of whether
230 these are organic or non-organic soils. However, we observed that the isotope associated
231 with the higher count (i.e., ^{40}K) is generally the most reliable.
232
233 The experimental set-up, which is illustrated in Fig. 1c, is based on the initial, snow-free
234 measurement of the number of counts for ^{40}K or ^{208}Tl per period of time, which would be
235 later decreased by the presence of the snowpack. Typically, 300 000 and 60 000 counts
236 per 24 hours for ^{40}K and ^{208}Tl, respectively, are suggested as minimal values to provide

237   accurate SWE measurements (CS725 Snow Water Equivalent Instruction Manual, 2017,
238   Campbell   Scientific   [Canada]   Corporation,   Edmonton,   AB;
239   https://s.campbellsci.com/documents/ca/manuals/cs725_man.pdf). The observed rate
240   of soil emission at each site allows the operator to define the minimum sampling time
241   frequency. Seeding experiments conducted using potassium fertilizer show potential for
242   increasing potassium counts that are measured by the CS725 by up to 80% at sites where
243   low counts are found (Wright et al., 2011). As is the case for ground-pointing CRNP,
244   measuring the base-line signal of the electromagnetic energy emanating from the ground
245   prior to the first snowfall is a critical step in signal processing, given that it also depends
246   upon soil moisture (SM) during the winter and spring periods. SM attenuates the natural
247   dry-ground emission, resulting in an overestimate of SWE during signal processing when
248   SM increases. Based upon 10+ years of experience with a large GMON network that is
249   deployed in Quebec, Canada, it has been shown that in most cases, SM does not vary
250   substantially during the winter season. It can be considered constant, thereby simplifying
251   mathematical equations used in calculating SWE (Choquette et al., 2013; Ducharme et al.,
252   2015).
253
254   The CS725-Campbell GMON sensor has been the subject of a detailed performance
255   analysis within the framework of the WMO Solid Precipitation Intercomparison
256   Experiment. SPICE (Smith et al., 2017). Moreover, since the device is sensitive to water
257   contained in soils, it can be successfully used to estimate soil moisture during snow-free
258   seasons. An operational GMON network, with a sampling frequency of 6 h, is actually
259   deployed across the southern part of Québec and Labrador, northeastern Canada (45-
260   55°N); it accounts for 114 stations in operation that are dedicated to water resource
261   forecasting (Alexandre Vidal, Hydro-Québec, personal communication, November 2020).
262   Also, these continuous measurements from the GMON Quebec network are
263   demonstrably very useful for validating the assimilation of microwave observations into
264   a snow model (Larue et al., 2018). Recently, GMON has also demonstrated its robustness
265   in a research project on seasonal snow monitoring from a station that was installed at
266   4962 m asl in the Nepalese Himalayas (Langtang Valley) to quantify the evolution of SWE
267   (Kirkham et al., 2019).
268
269   2.3 FMCW radar (FMCW-Radar)
270   The principle of frequency-modulated continuous-wave (FMCW) radar has been well
271   known since the 1970s (see the review by Peng and Li, 2019 and by Pomerleau et al.,
272   2020) and has been popularized for snow studies since Koh et al. (1996), Marshall et al.
273   (2005), and Marshall and Koh (2008), among others, were published. FMCW-Radar is an
274   active system design for distance measurements. The radar emits a wave at variable
275   frequencies that are centered on a reference frequency. When the radar receives a return
276   from a target, the frequency difference between the emitted and reflected signals is
277   measured (Fig. 1d). Since the frequency change rate is known, the time between the
278   emission and the reception of the echo can be measured from which the radar–target
279   distance is calculated.
280

281 The principle of SWE retrieval is based on the time measurement of wave propagation in
282 the snowpack that is proportional to the snow refractive index (square of permittivity),
283 which changes the wave-speed propagation. As the refractive index of snow can be linked
284 to its density (Tiuri et al., 1984; Mätzler, 1986; Pomerleau et al., 2020), SWE can be
285 retrieved knowing the snow depth. The experimental set-up is shown in Fig. 1d and
286 illustrated in Fig. 2e.

288 Two main FMCW radar specifications are required for SWE measurement: the radar
289 central frequency and its bandwidth that is scanned. The central frequency specifies three
290 parameters: a) the loss in signal strength of an electromagnetic wave that would result
291 from a line-of-sight path through free space (the higher the frequency, the greater the
292 loss); b) its penetration depth (the higher the frequency, the less penetration power it
293 has); and c) its sensitivity to liquid water content in the snowpack. The bandwidth
294 specifies the distance resolution and, thus, the precision: the wider the bandwidth, the
295 lower the resolution. There is negligible frequency dependency of the snow refractive
296 index (n'), which governs wave propagation in the snowpack. The refractive index (n') is
297 linked to snow density (ρ) by a linear relationship: $n' = 8.6148 \cdot 10^{-04} \rho + 9.7949 \cdot$
298 10^{-01} (Pomerleau et al., 2020).

300 For snow studies, several FMCW radars with different frequencies and resolutions are
301 used, such as those common at the X-band (10 GHz), operating over 8–12 GHz (Ellerbruch
302 and Boyne, 1980; Marshall and Koh, 2008). They provide a vertical resolution on the order
303 of 3 cm. In contrast, L-Band FMCW radar (1.12–1.76 GHz) allows greater penetration but
304 suffers from reduced vertical resolution (Yankielun et al., 2004). Multiband band FMCW
305 radar have also been developed (Rodriguez-Morales et al., 2014), such as an L/C-band (2–
306 8 GHz) that was used to successfully retrieve snow depth (Fujino et al., 1985), a C/Ku (8–
307 18 GHz) large wideband FMCW radar that is capable of detecting crusts as thin as 0.2 mm
308 within the snowpack (Marshall and Koh, 2005), or the improved (C-, X-, and Ka-band)
309 radar (Koh et al., 1996). Operating frequencies of commercial, low-cost radar systems,
310 such as those that are adopted for automotive radar systems (Schneider, 2005), are now
311 available for K-band (24 GHz) and W-band (77 GHz) applications.

313 The availability of such new types of lightweight and very compact 24-GHz FMCW radar
314 systems has motivated our research group to assess their ability to monitor the SWE
315 continuously and autonomously (Fig. 2e) (Pomerleau et al., 2020). The FMCW-Radar that
316 is used is centered on 24 GHz (K-band), scanning over (23–25.5 GHz), i.e., with a
317 bandwidth of 2.5 GHz that provides a resolution of 6 cm in the air (IMST sentire™, IMST,
318 Kamp-Lintfort, Germany; http://www.radar-sensor.com/). These specifications appear to
319 be a good compromise between penetration and resolution capabilities for SWE
320 estimation, while keeping the sensor affordable, light and compact, with low power
321 consumption. The radar penetration depth (δPr) of dry snow significantly decreases with
322 density following a power law, which varies with temperature (see Fig. A2, Pomerleau et
323 al., 2020). At T = 0 °C, δPr decreases from 6.78 to 4.81, 3.26 and 2.05 m for respective
324 snow densities of 150, 200, 275 and 400 kg m^{-3} (Pomerleau et al., 2020). Wet snow

325 drastically reduces δPr, given that liquid water strongly absorbs the radar signal, leading
326 to high reflectivity at the air/wet snow interface and weak transmissivity. For example,
327 the two-way radar penetration depth decreases abruptly from 2 m for dry snow at a
328 density of 400 kg m^{-3} to 0.05 m for wet snow with 0.5% of liquid water content. It should
329 be noted that this strong sensitivity to wet snow allows the radar to precisely detect the
330 onset of snowpack melt, a benefit that is discussed in Sect. 4.
331
332 One of the main interests of this approach is its potential capacity to estimate SWE from
333 a small remotely piloted aircraft (RPA). Over the Arctic, snow cover that can be
334 characterized by a two-layer snowpack structure, and assumptions can be made on its
335 mean refractive index, thereby allowing bulk SWE to be estimated (work in progress). Hu
336 et al. (2019) also showed the usefulness of imaging FMCW synthetic aperture radar
337 onboard the RPA. Several studies have also shown the potential of FMCW radar for
338 different applications, such as avalanche studies (Vriend et al., 2013; Okorn et al., 2014;
339 Laliberté et al., 2021), snow stratigraphy based on successive FMCW echo analyses
340 (Marshall and Koh, 2005; Marshall et al., 2007), snowpack tomography (Xu et al., 2018),
341 and ice thickness monitoring (Yankielun et al., 1993; Gunn et al., 2015). Pomerleau et al.
342 (2020) obtained highly accurate measurements of lake ice thickness using the 24 GHz
343 FMCW radar, with a root-mean-square difference (RMSD) of 2 cm accuracy up to ≈1 m ice
344 thickness (derived from 35 manual in situ measurements).
345
346 2.4 GNSS receivers (GNSSR)
347 The principle of SWE retrieval based on Global Navigation Satellite System (GNSS)
348 receivers is to use the signals that are emitted by the GNSS satellite constellations, and
349 relate the carrier phase change that is induced by the delay caused by the snowpack at
350 ground level. With two static receivers (standard GNSS antennas), i.e., one placed under
351 the snow and the other above the snow, both signals that are measured under dry-snow
352 conditions can be compared and SWE derived (Fig. 1e) (Henkel et al., 2018). Comparing
353 GNSS signal attenuation measurements between the two antennas (below and above the
354 snowpack) also permits the retrieval of Liquid Water Content (LWC) of the wet snow
355 (Koch et al., 2019).
356
357 This relatively recent and novel approach has been validated (Koch et al., 2019; Apple et
358 al., 2020) and is now commercialized by VISTA Remote Sensing in Geosciences GmbH,
359 Munich, Germany (SnowSense©, https://www.vista-geo.de/en/snowsense/). Snow
360 depth retrieval was made operational since a longer time that is based on interferometric
361 reflectometry of GNSS signals became available (see Larson et al. 2009; Larson, 2016).
362 GNSSR satellites operate at 1.575 and 1.609 GHz. The experimental set-up is described in
363 Fig. 1e, based on a low cost and lightweight system. In this study, we used the SnowSense
364 system for monitoring SWE and LWC throughout a winter, together with other sensors
365 (see Results Sect. 3). Our own system is shown in Fig. 2d.
366
367 Another promising way to monitor SWE, which is based on the same principle of GNSS, is
368 the use of powerful satellite transmissions as illumination sources for bistatic radar. This

369   so-called "Signals-of-opportunity (SoOp)" approach covers a wide range of frequencies,
370   such as emissions from United States Navy Ultra High Frequency (UHF) Follow-On (UFO)
371   communication satellites in P-Band frequencies (between 240-270 MHz). From two P-
372   band antennas (one direct and one reflected), Shah et al. (2017) demonstrated the
373   feasibility of retrieving SWE using the phase change in reflected waveforms, which is
374   linearly related   to the change in SWE. These methods were not included in this
375   review since they are still in the development stage and not sufficiently mature to be
376   operational.

377

378

379   **3. Results: examples of comparisons**

380

381   Continuous and simultaneous recordings of the different instruments on the same site
382   were conducted to analyze their behavior in terms of their temporal evolution. In situ
383   measurements were also used to compare the data between them. From these data,
384   which were completed by a literature review of experiments using these same
385   instruments, estimates of their respective accuracies are discussed (Sect. 3.4).

386

387   3.1 Experimental sites and validation measurements
388   We compared the four instruments at two snow research stations that were located in
389   Québec (Canada). The first was the SIRENE site (Site Interdisciplinaire de Recherche en
390   ENvironnement Extérieur), which is situated on the main campus of the Université de
391   Sherbrooke in a temperate forest environment (45.37°N, -71.92°W, 250 m asl) (Fig. 2d).
392   The second site is the NEIGE-Forêt Montmorency (NEIGE-FM) research station. The
393   instruments were located in an open area (Fig. 2e) of the Montmorency experimental
394   forest (47.32° N; -71.15° W, 640 m asl) of Université Laval (Quebec City), which is in the
395   boreal forest. The NEIGE-FM snow research station is part of the World Meteorological
396   Organization (WMO) Global Cryosphere Watch (GCW) Surface Network CryoNet (WMO
397   ID: 71212) (WMO, 2015).

398

399   Two methods were used to obtain in situ manual SWE measurements in the vicinity of
400   the four SWE-systems: the snowpit (SP) approach; and snow-tube core samplers (see
401   Kinar and Pomeroy, 2015). The SP-based SWE values (in mm = kg m^{-2}) were derived from
402   vertical continuous density profiles, which were determined by weighing snow samples
403   at a vertical resolution of 5 cm (height of the density cutter). Assuming an accuracy of
404   density cutter measurements of about 9% (Proksch et al., 2016), the mean relative SWE
405   accuracy can be estimated to be of 10–12%. SWE estimates were also obtained by
406   weighing the extracted core sample of known diameter (Ø) and length using a coring
407   tube. In this study, the core sampling was performed using three different snow tube
408   models, which were averaged: "Carpenter" (Federal standard sampler, 3.7 cm Ø tube),
409   the Hydro-Quebec snow tube (12.07 cm Ø), and an in-house Université Laval snow tube
410   (15.24 cm Ø). The accuracy of tube core sampling that we carried out on snowpack up to
411   600 mm SWE with large tubes is of the order of 6% (Brown et al., 2019). Such accuracy is
412   difficult to define, as discussed in Sect. 3.4. Furthermore, as manual measurements

413 cannot be taken at the same location during a given winter period, this could generate
414 uncertainty when compared to a fixed instrument, due to small-scale spatial variability of
415 SWE and surface roughness.

417 The snowpack properties were derived continuously from GMON and CRNP systems
418 throughout the entire winter season of 2008-2009 (Fig. 3) and from GMON, FMCW-Radar
419 and GNSSR systems in 2017-2018 (Fig. 4). In addition to SWE measurements, continuous
420 automatic snow depth measurements were performed using an acoustic sensor
421 (Campbell Scientific, SR50AT-L), and manually with a graduated probe around the
422 sampling sites. LWC measurements were derived from GNSSR (Fig. 4). Air temperature (T)
423 at 2 m height and total daily cumulated precipitation (Global Water tipping bucket rain
424 gauge) were recorded at the SIRENE site; a threshold of T = 0 °C was used to separate
425 solid and liquid phases (Fig. 3). In this section, we present comparisons between these
426 sensors with in situ validation data measured as close as possible to the automatic
427 instruments, and their accuracy, which was also based on literature values and other
428 measurements that we carried out (not shown), is analyzed in Table 2.

430 3.2 Comparison of GMON- and CRNP-derived SWE seasonal evolution
431 Figure 3 shows the SWE evolution of a shallow snowpack (maximum snow depth of 56
432 cm) at the SIRENE site that was derived from GMON and CRNP sensors throughout the
433 winter season of 2008-2009. The CNR probe that was used was the same as the French
434 EDF probe placed on the ground (Paquet et al., 2008) and installed at about 5 m distance
435 from the GMON footprint. The CNRP counts were accumulated over 1 hour and
436 normalized by an identical probe that was installed nearby just above the snow surface.
437 The GMON counts were accumulated over 6 hours, and only ^{40}K counts were considered
438 (TI counts were similar, but not shown). The GMON sensor, which was installed on a 2 m
439 mast above the surface, was calibrated to take into account the soil moisture prior to
440 snowfall accumulation. In Fig. 3, we have plotted daily mean values of the CRNP and
441 GMON data. In situ measurements were derived from snowpit measurements that were
442 taken around these two instruments at a maximum radius of 20 m.

444 Results show that GMON and CRNP evolve similarly over the winter, with GMON SWE
445 being slightly higher after the first winter month (SWE > 50 mm). This difference occurred
446 after a pronounced melting spell (29-30 December 2008) and is explained by the water
447 that has accumulated on the ground under the GMON and not on the CNRP. The moisture
448 beneath the GMON formed a significant ice layer that lasted all winter. Precipitation
449 (snowfall and rain) is also plotted, showing how GMON and CNRP develop with each
450 event. For that given winter, rain-on-snow events were frequent, leading to moisture
451 accumulation on the ground. Note also that at the end of the winter, there was ice that
452 had not yet melted and water accumulation under the GMON, leading to a significant
453 overestimation of GMON SWE when there was no more snow on the ground after March
454 20, 2009. The accuracy measurements are discussed in Sect. 4.2.

456
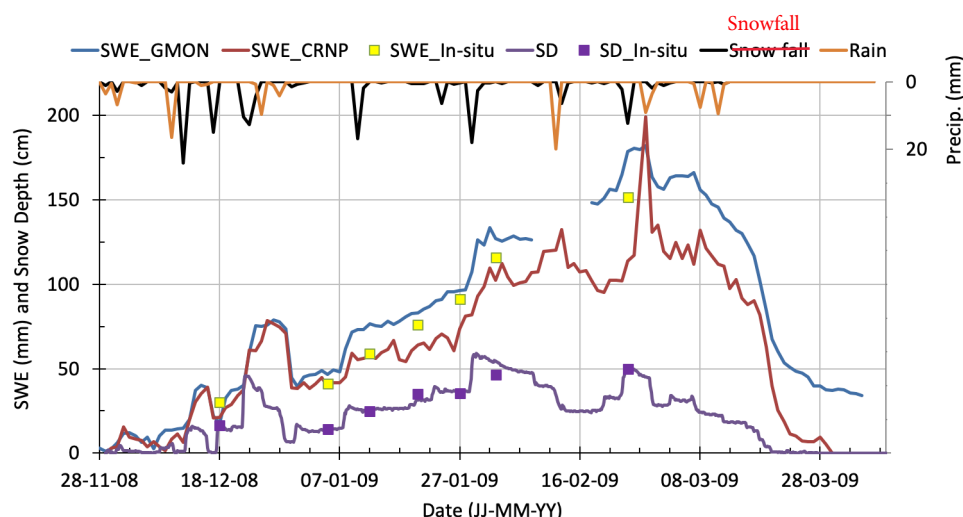
457 Figure 3. GMON- and CRNP-derived snow water equivalent (SWE, mm), snow depth (SD,
458 cm), and recorded daily solid and liquid precipitation (Precip., mm, right hand scale), in
459 comparison to validation data (in situ) at the SIRENE site for the winter season of 2008-
460 2009. Continuous SD measurements (purple line) are from SR-50 and SD_in situ
461 measurements (purple square) are from snowpits. Open yellow squares correspond to
462 manual in situ SWE measurements.

463

464

465 3.3 Comparison of GMON-, Radar- and GNSSR-derived SWE seasonal evolution

466 Figure 4 shows the SWE evolution that was measured by the three instruments, i.e.,
467 GMON (^{40}K counts only), FMCW-Radar and GNSSR, which had been placed in close
468 proximity to one another at the NEIGE-FM research station for the winter season of 2017-
469 2018. Snow depth was monitored up to 120 cm, corresponding to 500 mm SWE maximum
470 at the end of April.

471

472 The three instruments were compared to manual in situ measurements that had been
473 derived from SP (red squares) and core (red triangles) approaches in Fig. 4. We
474 distinguished the two methods (SP and snow tube) because they exhibit significant
475 differences, with a RMSD of 33 mm (12%). These discrepancies are the result of two
476 problems: 1) SWE spatial variability; and 2) the method that was used, since the design of
477 snow tubes and cutters has some influence on sampling errors and bias (Goodison et al.,
478 1987). Therefore, accuracy analyses (Sect. 3.4) were performed considering manual SP as
479 the reference because the SP approach was used for both experiments.

480

481
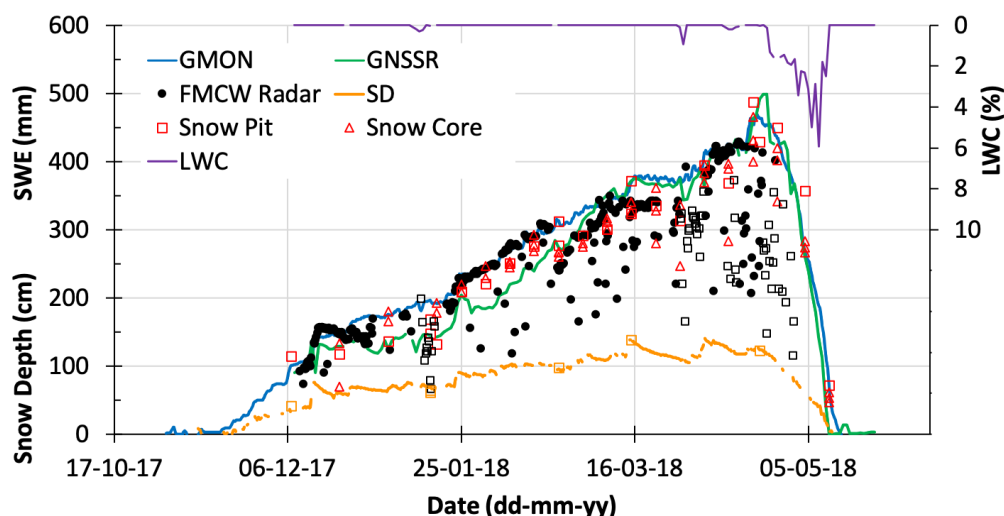
482
483 Figure 4. GMON- (blue line), FMCW Radar- (black closed circles) and GNSSR-derived
484 (green line) snow water equivalent (SWE, mm), snow depth (orange line for SR50AT-L
485 data and orange open squares for in situ data) (SD, cm) and GNSSR-derived Liquid Water
486 Content (LWC, % volumetric, purple line, right scale), in comparison to in situ snowpit
487 (open red square) and snow core (open red triangle) SWE measurements at the NEIGE-
488 FM site for the winter season of 2017-2018. For FMCW-Radar data (in black), plain circles
489 are for dry snow, while open squares correspond to wet snow from air temperature
490 measurements.
491
492 The continuous simultaneous recordings from the different instruments permit temporal
493 evolution analysis (Fig. 4). While GMON SWE values regularly increase up to 465 mm on
494 19 April 2018, the FMCW-Radar data appears noisier and must be smoothed to eliminate
495 outliers that show underestimated SWE values. These points are mainly due to incorrect
496 detection of the peak of the radar echo on the ground (snow-ground interface),
497 sometimes with low amplitude, and which can be filtered with improved data quality
498 processing of raw recording (Pomerleau et al., 2020). In particular, all data acquired under
499 wet snow conditions (open black squares, Fig. 4) are obviously underestimated as
500 expected, because of radar wave absorption by liquid water in the snowpack. Compared
501 to the GMON, the GNSSR signal increases with values lower than the GMON until the mid-
502 March and continue to evolve with similar absolute values until the SWEmax was reached
503 on 23 April 2018 with a SWE value of 499 mm. The behavior of the three instruments,
504 showing ~~slightly~~ different patterns of snow evolution, remains always close to in situ
505 observations. It should be noted that in Fig. 4, there is a small difference (+4 days)
506 between the end of snow cover that was recorded with GNSSR (11 May 2018) compared
507 to GMON (14 May 2018). The GNSSR sensor is not sensitive to soil moisture, while GMON
508 is, despite the instruments being located on a well-drained sandy site (NEIGE-FM site). In
509 the case shown here, the end of snowmelt is well captured by both instruments. The

510 accuracy between instruments is analyzed in Sect. 3.4, including a second winter season
511 of continuous measurements at the NEIGE-FM site (2016-2017, Pomerleau et al., 2020).
512
513 GNSSR also measures the Liquid Water Content (LWC) of snow (purple line in Fig. 4). The
514 non-zero LWC values correspond well to positive air temperatures that were recorded at
515 this site, and also to the drop in FM-Radar measurements (open black squares).
516
517 3.4 ~~Accuracy analysis~~
518 It is challenging to compare the accuracy of several instruments, given that there is no
519 absolute reference for estimating SWE (see Kinar and Pomeroy, 2015). In situ manual
520 measurements are themselves subject to error, with varying precision depending upon
521 the method that is being used. Errors are incurred that depend upon the types of density
522 cutter, tube diameter, sampling quality that is operator dependent, and ice lenses in the
523 snowpack, among other sources. This is a long-debated topic, with no actual established
524 international standard protocol (Work et al., 1965; Goodison et al., 1981, 1987; Kinar and
525 Pomeroy, 2015). For example, the standard protocol from Environment and Climate
526 Change Canada is to attain five to ten measurements along a pre-determined survey line
527 of about 150 to 300 m using a translucent plastic ESC-30 sampler (6.2 cm Ø, which is
528 commonly employed in Canada) (Brown et al., 2019). The accuracy of the tube core
529 sampler for medium snowpack (up to ~600 mm SWE) and with large tubes (Ø ~> 6 cm)
530 is about 6%; for higher SWE requiring smaller diameter tubes, it is around 10% (Work et
531 al., 1965; Goodisson et al., 1987; Dixon and Boon, 2012; Brown et al., 2019). Moreover,
532 because manual measurements cannot be taken at the same location during a given
533 winter period, uncertainty can be introduced by well-known local SWE spatial variability
534 that can occur at fine scales around the sensors. Such variability depends upon several
535 factors, such as the region and the environment (Arctic area, aspect and slope in
536 mountainous areas, for example), the micro-topography and roughness, the vegetation,
537 and snow redistribution by the wind (Clark et al., 2011; Bormann et al., 2013; Rutter et
538 al., 2014; Meloche et al., 2021; Royer et al., 2021). Furthermore, temporal variability of
539 snowpack properties during the winter requires regular validation measurements
540 throughout the season.
541 The sensor accuracies were evaluated from ~~results that have been previously shown~~
542 ~~(Sect. 3.2 and 3.3) and~~ from published studies at other experimental comparison sites.
543 These other sites are: the Weissfluhjoch high-alpine site near Davos, Switzerland (46.83°
544 N, 9.81° E, 2 536 m asl); Sodankylä, Finland (67.37° N, 26.63° E, 185 m asl); Caribou Creek,
545 SK, Canada (53.95° N, -104.65°W, 519 m asl); and Fortress Mountain ski area, Kananaskis
546 Country, Canadian Rocky Mountains, AB (50.82° N, -115.20° W, 2 330 m asl).
547 We also conducted a series of ~~manually~~ FMCW-radar measurements over dry snowpack
548 and compared them with in situ SWE measurements over a wide range of conditions
549 (snow depth and density) in boreal forest (47° N, 18 points), subarctic taiga (54–56° N, 32
550 points) and Arctic tundra (69° N, 28 points) environments along a northeastern Canadian
551 transect (Pomerleau et al., 2020). The results are reported in Table 2.
552

553 Table 2 summarizes the accuracy of each instrument and protocol (five cases: CRNP in
554 and above ground, GMON, FMCW-Radar and GNSSR) in relation to in situ manual
555 measurements (snowpit method), and against snow pillow data that were considered as
556 reference measurements by the authors of the publications consulted. Even if this
557 mechanical method is well known and proven for a long time, the snow pillow can
558 sometimes generate large uncertainties when bridging processes occur that are linked to
559 freeze–thaw cycles leading to disconnection of the weighing mechanism from the
560 overlying snowpack (Kinar and Pomeroy, 2015). In Table 2, when known, the accuracy
561 was defined by the root-mean-square difference (RMSD) between an instrument and a
562 given reference, and by a linear regression that was defined by the coefficient of
563 determination (R^2), the slope and the intercept. The number of points is also given.
564
565 Table 2 here
566
567 The accuracy analysis does not allow us to determine the instrument that has the best
568 accuracy, due to the diversity of experimental conditions, including the range of SWE, the
569 number of experimental sites and point measurements, and analyses that are performed
570 over one or several seasons. It appears that all of the five methods show remarkably good
571 performance, with an average RMSD against in situ snowpit manual measurements on
572 the order of 33 ± 11 mm, over a range of 14 to 48 mm, i.e., about 12% of mean SWE (Table
573 2). The mean regression is also significantly high (mean R^2 = 0.92 ± 0.07). Calculated
574 average slope is 0.976 ± 0.13, meaning that in general, the instruments slightly
575 underestimate SWE for higher SWE values compared to in situ measurements, even if this
576 is not always the case (Table 2). RMSD increases slightly when the analysis was performed
577 over a deep snowpack (0 – 1 000 mm) and decreases when compared to another
578 continuous instrument instead of in situ data (instrument vs GMON and instrument vs
579 snow pillow, average RMSD = 23 ± 10 mm, Table 2).
580
581 For the GNSSR instrument that allows the operator to differentiate dry from wet snow,
582 Koch et al. (2020) have shown that SWE RMSD is about 2.4-fold higher for wet snow than
583 for dry snow. They did not provide information on LWC uncertainty. In late winter 2021,
584 for very wet melting snow, we did a validation measurement using the WISe A2 Photonic
585 probe (snow liquid-water content sensor that is based on snow microwave permittivity
586 measurements; https://a2photonicsensors.com/wise/). GNSSR and in situ LWC values
587 were respectively 0.44 and 0.47 %, for respective SWE of 149 and 133 mm. The
588 uncertainty in wet SWE retrieval could result from approximations of the wet snow
589 refractive index that is used in the retrieval process, and which is very sensitive to LWC.
590 This aspect could probably be addressed by improved inversion.
591
592 The accuracy comparison in Table 2 must be weighted according to the analysis
593 conditions. The accuracy estimates can actually depend upon the number of points being
594 used and their distribution over time. High inter-annual variability of the snowpack state
595 (see Bormann et al., 2013; Lejeune et al., 2019) ideally would necessitate several years of
596 measurements over the winter. The accuracies of each GMON and CNRP instrument were

derived from huge data sets that were based on operational networks from the GMON Hydro-Quebec network in Canada and the Alps' EDF network for the CNRP, respectively, with a very large number of samples taken over several years of experiments and from multiple sites. The accuracy of the GMON that is given by the manufacturer is ± 15 mm for SWE < 300 mm and ± 15% for SWE of 300-600 mm, which is probably rather conservative. The accuracy of the SnowFox sensor (CRNP) that has been provided by the manufacturer (5-10%) must be confirmed. The GNSSR approach has recently been the subject of two different comparative analyses showing very promising results (Henkel et al., 2020; Koch et al., 2020), which were confirmed by our own results. Over a full season, we obtained an excellent relationship between GNSSR and in situ manual measurements (RSMD = 11%, Table 2) and compared with GMON (RMSD = 34 mm, 12%, SWE_{GNSSR} = 1.126 SWE_{GMON} - 59.3, R^2 = 0.97, 153 days).

4. Strengths and Weaknesses of Instruments

In this section, we review the advantages and drawbacks of each of the instruments that are presented, summarized in Table 3. This analysis is based on our experience, on instrument and protocol performances (Sect. 3), and a literature review on experimental results of measurements that were carried out with the same approaches. We only consider these field sensors for SWE measurements in terms of their continuous and autonomous capacities, from the perspective of an operational networking context, including criteria on price, low maintenance and relatively easy installation without requiring heavy infrastructure. The four instruments we analyzed are: CRNP with two experimental setups, i.e., instrument in the ground and above the snow; GMON; 24-GHz FMCW-Radar; and GNSSR (see Table 1 for acronyms and Fig. 1 for the experimental setup). They are all capable of working on batteries and solar panels, by adjusting, if necessary in certain cases, the measurement protocol, i.e., by reducing the frequency of acquisition and on-board data processing. Nine criteria were considered (Table 3): the SWEmax capability; other measured parameters; whether ancillary data were required for SWE retrieval; the temporal sampling rate, i.e., whether they were capable of continuous measurement capability; the footprint of the sensor; the main strength of the approach; their critical drawbacks; their relative prices; and the possibility of other applications.

Table 3 here

To complement the main criteria that are presented in Table 3, we include the following additional considerations, which are reported in the literature, by order of presentation rather than order of merit or not:

- CRNP approach is based on neutron component that has absorption mean free path about an order of magnitude larger than that for gamma radiation. This makes it the most efficient system for very deep snowpack analysis (Paquet et al. 2008). Measurements over a snowpack of up to 2000 mm SWE were performed using the

641   SnowFox sensor at the UC Berkeley Central Sierra Snow Lab in Soda Springs, CA (2 120
642   m asl; https://vcresearch.berkeley.edu/research-unit/central-sierra-snow-lab). The
643   cost of the CRNP-based sensor that is manufactured by Hydroinnova (SnowFox or CRS-
644   1000/B, Hydroinnova, Albuquerque, NM) is about 16 500 USD for full setup (11 000
645   USD for sensor only). As previously mentioned, ancillary sensors (atmospheric
646   humidity and barometric pressure sensors) must be added.

647 -   CRNP is inherently less sensitive to interference from vegetation compared to systems
648   that are based on lower frequencies (FMCW-Radar and GNSSR). This is in part because
649   the attenuation coefficient for fast neutrons ($\sim$0.01 m^{-2} kg in water, Murray and
650   Holbert, 2020) is an order of magnitude smaller than the analogous attenuation
651   coefficient in vegetation for GNSS microwaves (1.5 GHz) (e.g., Wigneron et al., 2017).
652   Moreover, vegetation can itself be a significant source of electromagnetic emissions
653   (Larson et al., 2014; Wigneron et al., 2017), but not neutron emissions.

654 -   The instruments pointing toward the soil, CRNP and GMON above the surface, can be
655   affected by heavy rainfall on snow leading to erroneous SWE estimates that are due
656   to the occurrence of ponding water below the snow (Bogena et al., 2020). Installation
657   on well-drained soils can mitigate these effects.

658 -   Counter-based sensors such as CRNP and GMON need to accumulate enough counts
659   for reliable SWE estimates. Thus, it may be necessary to accumulate the counts over
660   an adjusted period of time (several hours, depending on the case), so that the
661   measurement is not continuous. This can prevent accurate detection of short events,
662   sudden heavy snowfalls, for example. For the GMON, depending on the type of soil at
663   the measurement site, gamma ray emissions may not be sufficient and could require
664   a longer integration period, as is the case for sites with thick organic soil layers. It is
665   possible to enrich gamma emissions by using bags or pipes of potassium-rich fertilizer,
666   thereby maintaining a shorter integration time. We achieved success with this
667   approach at the NEIGE-FM site, yielding significantly higher count strengths (Fig. 2g)
668   (Wright et al., 2011). .

669 -   FMCW-Radar. With this technique, as previously stated, penetration depth strongly
670   depends on the measurement frequency. Generally, high frequency instruments
671   result in higher resolution measurements, but these are also affected by greater signal
672   attenuation, i.e., by a reduced depth of penetration.

673 -   GNSS electromagnetic waves can be attenuated under the forest canopy, as the forest
674   transmittivity at 1.5 GHz is not negligible (Wigneron et al., 2017). Yet, because we
675   normalized the signal beneath the snow against the one acquired above the
676   snowpack, when both antennas were placed under the canopy, this effect should not
677   alter retrieval.

678 -   GNSSR is not well suited to very steep mountainous terrain (e.g., deep-valley
679   bottoms), given that a rather wide sky-view factor is needed by the instrument, ~~but~~
680   this view can be limited in such environments, depending on slope and location (Koch
681   et al., 2019).

682

683 The main conclusions that emerge from Table 3 and the aforementioned remarks are the
684 following, recalling that each approach has its own advantages and limitations (by order
685 of presentation rather than by order of merit):

- 686 • CRNP on the ground: This is the most efficient system for very deep snowpack (≥ 5
687 meters of snow depth), as is the case in mountain environments or northerly areas
688 that are witness to winter lake-effect snowfall. It has good accuracy over a large range
689 of measurements, typically 12% for 0-2000 mm SWE. The main drawback is that it
690 requires auxiliary sensors for SWE retrieval (synchronous data from a reference
691 station and atmospheric pressure and humidity measurements). This is a robust and
692 mature approach, as proven by the French EDF experience (Gottardi et al., 2013;
693 Lejeune et al., 2019); however, it based on a system that is yet to be exploited
694 commercially. The alternative sensor is the SnowFox system
695 (https://hydroinnova.com), which is relatively new and still needs to demonstrate its
696 robustness.
- 697 • CRNP above the snow: The most interesting system for measuring SWE over a large
698 footprint, but it is limited to shallow snowpacks. It is the only approach that can
699 provide an integrated spatial measurement. Schattan et al. (2017) estimated the
700 theoretical winter footprint over snow, which they defined as the distance from
701 where neutrons originate. They found that 86%, 63% and 50% of neutrons originate
702 within respective distances of 273, 102, and 49 m. In practice, the authors found that
703 the average footprint during the season, based on measurements over almost three
704 snow seasons, was estimated to be around 230 m. This approach also needs thorough
705 calibration for each site in terms of soil moisture corrections, which can be difficult
706 over a large area.
- 707 • GMON: This is one of the most mature instruments for snowpack that is not too deep
708 (max 2.5 to 3 m snow depth), with an interesting medium footprint (2-3 m). Yet, it
709 needs systematic site calibration for soil moisture characterization, which can
710 increase the uncertainty of measurements, particularly at the end of the season when
711 the soil is potentially saturated. It is the most expensive of the four instruments
712 (around 20 000 $CAD). This system has proved its robustness and accuracy within the
713 operational Hydro-Quebec Canadian network over a wide variety of environments for
714 almost 10 years (Choquette et al., 2013).
- 715 • FMCW-Radar: its weak point is its limitation in measuring the SWE of wet snow. Yet,
716 the instrument is very useful for dry snowpack characterization, in terms of
717 stratigraphy or for avalanche studies, and also for detection of snowmelt events.
718 Moreover, it is not expensive (800 Euros). As it is very light weight and compact, one
719 of its strengths is its potential capability to retrieve SWE from remotely piloted aircraft
720 above arctic snowpacks.
- 721 • GNSSR: The potential of the GNSSR approach is strong, given its capability of
722 measuring SWE, SD and LWC with high accuracy. For SWE retrieval, its performance
723 remains very good (~10% in the range of 0-1000 mm) and has the capacity of
724 measuring deep snowpack (up to 5 m snow depth). It is an inexpensive (7 000 Euros),
725 light and compact system. SWE accuracy for wet snow has yet to be improved.

726

5. Conclusions

In this paper, we evaluated four types of SWE sensors that have all reached a certain level of maturity enabling deployments of autonomous networks. These include the Cosmic Ray Neutron probe (CRNP), the Gamma Ray Monitoring (GMON) sensor, the frequency-modulated continuous-wave radar at 24 GHz (FMCW-Radar), and the Global Navigation Satellite System receiver (GNSSR) (see Table 1). This new generation of light, practical and low-cost systems that are based on electromagnetic-wave measurement are now commercially available. The GMON is already operationally used in Québec, Canada, for hydrological purposes (Hydro-Québec).

The analysis of their performances that are summarized in Tables 2 (accuracies) and 3 (pros and cons) show that each approach has its strengths and weaknesses. The synthesis of their advantages/disadvantages shows that:

- CRNP that is placed in the ground beneath the snow is the only system capable of measuring very deep snowpacks. This approach is based on measurements of natural cosmic ray fluxes, which are variable in time, and unfortunately needs complementary atmospheric measurements (temperature, pressure and atmospheric humidity) at each site for correcting the signal and must be normalized against a nearby reference site (available worldwide). The footprint of this sensor is quasi-punctual, a drawback that can be overcome by placing the sensor above the snow, but at the expense of its singularly diminished capacity (max ~150 – 300 mm SWE).
- The GMON has very good accuracy below 12%, but it is limited to snow covers that are not too thick (up to ~800 mm SWE). Its 2-3 m diameter footprint is a useful advantage, but this approach needs systematic site calibration for soil moisture characterization. Also, it is the most expensive of the four instruments that were considered.
- The FMCW-Radar is not recommended for automatic SWE monitoring, as it is limited to dry snow. Yet, it is very sensitive to wet snow, which makes it a very useful sensor for snow melt detection (wet avalanche forecasting, for example).
- The GNSSR permits the simultaneous retrieval of three key snowpack parameters: SWE, snow depth and Liquid Water Content. Given that the sensor is a low cost, light and compact option, this approach appears to have the strongest potential for a wide range of applications.

The requirement of automatic instrumentation networks for snow water equivalent monitoring to improve seasonal snowpack retrievals is important for several applications. For example, dense spatially distributed networks of SWE instruments are needed in remote and mountainous areas, for operational water resource and flood management over snow-driven watersheds, for calibrating satellite-derived SWE information, or for winter transportation safety. This review of continuous-monitoring SWE sensors is intended to help researchers and decision makers choose the one system that is best suited to their needs.

Acknowledgements

We acknowledge all ~~of~~ the students who have contributed to the field measurements, including Amandine Pierre, Maxime Beaudoin-Galaise and Benjamin Bouchard from Université Laval, and Patrick Pomerleau, Fannie Larue and Alex Mavrovic from Université de Sherbrooke. We thank, for their support, the staff from Forêt Montmorency and from the Université de Sherbrooke: Patrick Cliche, Patrick Ménard and Gabriel Diab. We also thank Alexandre Vidal, Hydro-Québec, and Vincent Fortin, Environment Canada and Climate Change (ECCC).

Funding:

This project was funded by the Natural Sciences and Engineering Research Council of Canada (NSERC), the Canadian Foundation for Innovation (CFI), Environment and Climate Change Canada (ECCC), and Fonds de recherche du Québec – Nature et technologies (FQRNT), Government of Quebec.

Conflict of interest:

The authors declare absolutely no conflicts of interest or business relationships with any of the manufacturers that are mentioned in this article. The mention of commercial companies or products does not constitute a commercial endorsement of any instrument or manufacturer by the authors.

Table 2 Accuracy analysis for the 4 systems considered. The Range measurement indicates the ~~highest~~ SWE (mm) value on which the analysis was performed. RMSD: Root Mean Square Difference. R^2 is the determination coefficient of the linear regression analysis. Pts: number of in situ manual samples. "-" means no information available

Sensor	Reference data	Range SWE (mm)	Accuracy RMSD (mm), R^2 (slope, intercept)	References, sites, number of points
CRNP in the ground	Manual snowpit	200	14 mm, R^2 = 0.96 (0.78, 8.5 mm)	This study (Fig. 3), 7 pts
	GMON	200	28 mm, R^2 = 0.89 (0.79, -3.9 mm)	This study (Fig. 3), 2008-2009 season
	–	-	5 – 10%	Hydroinnova communication[1]
	Manual snowpit	1700	–, R^2 = 0.98 (0.99, ~~2.8~~ mm)	~~Gotterdi~~ et al. (2013) EDF system, Alps and Pyrénées 320 year.sites, 1037 pts.
CRNP above the snow	–	-	5 – 10%	CRS-1000/B Hydroinnova communication[2]
GMON	Manual snowpit	500	34 mm (12%), R^2 = 0.93 (0.997, 17.1 mm)	This study (Fig. 3 and 4) and Pomerleau et al. (2020), SIRENE et NEIGE-FM, 64 pts
	Manual snowpit	200	40 mm, R^2 = 0.92 (1.16, 16.8 mm)	Smith et al., 2017, Sodankylä, Finland, 30 pts
	Manual snowpit	250	23 mm, R^2 = 0.90 (0.904, 27.5 mm)	Smith et al., 2017, Caribou Creek, Canada, 19 pts
	Manual snowpit	700	48 mm, R^2 = 0.92 (0.881, 32.4 mm)	Smith et al., 2017, Fortress Mountain, Canada, 8 pts
	Snow-pillow	200	–, R^2 = 0.95 (1.20, 14 mm)	Smith et al., 2017, Davos, Switzerland
	–	~~300~~ ~~600~~	±15 mm ±15%	Campbell Scientific CS725 manual[3]
FMCW-Radar 24 GHz	Manual snowpit	500	38 mm (14%), R^2 = 0.73 (0.80, 65.0 mm)	This study (Fig. 4) and Pomerleau et al., 2020, 46 pts, dry snow
	Manual snowpit	750	59 mm (30%), R^2 = 0.87 (0.98, 0)	Pomerleau et al., 2020, manual measurements, multi sites Northern Québec, Canada, 78 points dry snow
GNSSR	Manual snowpit	500	32 mm (11%), R^2=0.93 (1.05, -7.9 mm)	This study (Fig. 4), 18 points
	Manual snowpit	> 2000	± 15 mm	SnowSense Vista Inc. manual[4], good conditions
	Manual snowpit	700	23 mm, R^2 = 0.995 (0.98, 5.52 mm)	Henkel et al. 2018, ~~Davos~~, Switzerland
	Snow-pillow	700	11 mm R^2 = 0.999 (1.01, 1.97 mm)	
	Manual snowpit	1000	45 mm R^2 = 0.98 (0.98, 31.4 mm) 103 mm R^2 = 0.86 (0.88, 67.3 mm)	Koch et al., 2019 dry snow, 3 winters Koch et al., 2019 wet snow, 3 winters
	Snow-pillow	1000	30 mm R^2 = 0.99 (0.97, 30.5 mm) 72 mm R^2 = 0.93 (0.92, 65.0 mm)	Koch et al., 2019 dry snow Koch et al., 2019 wet snow

1 https://hydroinnova.com/_downloads/snowfox_v1.pdf, Hydroinnova, Albuquerque, NM

2 Hydroinnova, Albuquerque, NM; http://hydroinnova.com/snow_water.html

3 Campbell Scientific (Canada) Corporation, CS725 manual, https://s. campbellsci.com/documents/ca/manuals/cs725_man.pdf.

4 https://www.vista-geo.de/en/snowsense/

Table 3 Pro and Cons of the four systems that were considered for SWE monitoring. SM: Soil Moisture. FOV: Field-of-View. The approximate price is given (2021), subject to change according to exchange rate fluctuations.

Sensors	CNRP		GMON	FMCW-Radar 24 GHz	GNSSR
	CRNP on the ground	CRNP above the snow			
SWEmax	> 2000 mm	~150-300 mm	~800 mm	~1000 mm	> 1500 mm
Other measured parameters	-	SM	SM	Melt detection	SD, LWC
Other sensors needed	P, T_{air}, RH	P, T_{air}, RH	–	SD	–
Typical sampling rate	Discontinuous[a]	Discontinuous[a]	Discontinuous[a]	Continuous	Not strictly continuous[b]
Footprint	~1 m^2	20-40 ha (300 000 m^2)	FOV 60° Typically, 3 - 10 m^{2*}	FOV ±32.5° azimuth and ±12° elevation, 0.4 m^{2*}	~1 m^2
Price (US$)	Hydroinnova: 11 000 (sensor only) EDF: Not marketed (on request)[c]		16 600 (sensor only)	1 000 (radar and software[d])	8 550 (complete station[e])
Main advantage	Very deep snowpack	Large footprint	Medium footprint Deep snowpack	Medium footprint Deep snowpack Very light and compact Low cost	Very deep snowpack SD and LWC Low cost
Main inconvenience	SM issue Needs ancillary measurements	SM knowledge needed, Needs ancillary measures Shallow snowpack	SM knowledge needed	Dry snow only	Large sky view factor required
Other drawbacks	Cost EDF system not commercially available	Cost	Relatively expensive	Not turnkey Ice crust within the snowpack	SWE estimates for wet snow must be improved
Main applications, Capability (see text) Comments	Hydrology Network operational by EDF[c]	Hydrology, SM	Hydrology, SM Network operational by Hydro-Québec	SM, Stratigraphy, Avalanche, Melting monitoring Lake ice thickness RPA capability[f]	Hydrology, SM Avalanche, Melt monitoring

a Counts must be accumulated over a specified period, e.g. 6h, 12h, or longer. b GNSS signals must be averaged over a period of time for noise reduction; the typical measurement cycle: 1 per day (possibly up to 6 per day). c System based on a sensor that is not commercialized. d Software for sensor settings and reading/recording data, but not for SWE retrievals. e Subscription license required. f Remotely Piloted Aircraft capability.

* Depending on the height of the sensor on its support mast above snow, Field-of-View (FOV) given for 3 m mast.

References

For references related to a sensor, the name of the sensor has been highlighted in **bold.**

Alonso, R., Pozo, J.M.G.d., Buisán, S.T., and Álvarez, J.A: Analysis of the Snow Water Equivalent at the AEMet-Formigal Field Laboratory (Spanish Pyrenees) During the 2019/2020 Winter Season Using a Stepped-Frequency Continuous Wave Radar (SFCW), Remote Sens., 13, 616. https://doi.org/10.3390/ rs13040616, 2021. (**SFCW radar**)

Andreasen, M., Jensen, K. H., Desilets, D., Franz, T., Zreda, M., Bogena, H., and Looms, M.C.: Status and perspectives of the cosmic-ray neutron method for soil moisture estimation and other environmental science applications. Vadose Zone J., 16, 1–11. doi: 10.2136/vzj2017.04.0086, 2017. (**CNRP**)

Bissell, V.C., and Peck, E.L.: Monitoring snow water equivalent by using natural soil radioactivity. Water Resour. Res., 9, 885–890, 1973. (**GMON**)

Bogena, H.R., Herrmann, F., Jakobi, J., Brogi, C., Ilias, A., Huisman, J.A., Panagopoulos, A., and Pisinaras, V.: Monitoring of Snowpack Dynamics With Cosmic-Ray Neutron Probes: A Comparison of Four Conversion Methods. Front. Water, 2, 19, doi: 10.3389/frwa.2020.00019, 2020. (**CNRP**)

Bormann, K.J., Westra, S., Evans, J.P., and McCabe, M.F: Spatial and temporal variability in seasonal snow density, J. Hydrol., 484, 63–73, 2013.

Brown, R.D., Fang, B, and Mudryk, L.: Update of Canadian Historical Snow Survey Data and Analysis of Snow Water Equivalent Trends, 1967–2016, Atmosphere-Ocean, DOI: 10.1080/07055900.2019.1598843, 2019.

Brown, R.D., Smith, C., Derksen, C., and Mudryk,L. : Canadian In Situ Snow Cover Trends for 1955–2017 Including an Assessment of the Impact of Automation, Atmosphere- Ocean, DOI: 10.1080/07055900.2021.1911781, 2021.

Carroll, T. R.: Airborne Gamma Radiation Snow Survey Program: A user's guide, Version 5.0. National Operational Hydrologic Remote Sensing Center (NOHRSC), Chanhassen, 14, https://www.nohrsc.noaa.gov/snowsurvey/, 2001. (**GMON**)

Choquette, Y., Ducharme, P., and Rogoza, J.: CS725, an accurate sensor for the snow water equivalent and soil moisture measurements, in: Proceedings of the International Snow Science Workshop, Grenoble, France, 7–11 October 2013, 2013 (**GMON**)

Clark, M. P., Hendrikx, J., Slater, A. G., Kavetski, D., Anderson, B., Cullen, N. J., Kerr, T., Hreinsson, E. Ö., and Woods, R. A.: Representing spatial variability of snow water equivalent in hydrologic and land-surface models: A review, Water Resour. Res., 47, W07539, doi:10.1029/2011WR010745, 2011.

Desilets, D., Zreda, M., and Ferré, T.P.A.: Nature's neutron probe: Land surface hydrology at an elusive scale with cosmic rays, Water Resour. Res., 46, 1–7, 2010. (**CNRP**)

Desilets, D., and Zreda, M.: Footprint diameter for a cosmic-ray soil moisture probe: Theory and Monte Carlo simulations, Water Resour. Res., 49, 3566–3575, 2013. (**CNRP**)

Desilets, D.: Calibrating a non-invasive cosmic ray soil moisture probe for snow water equivalent, Hydroinnova Technical Document 17-01, doi:10.5281/zenodo.439105, 2017. (**CNRP**)

Dixon, D., and Boon, S.: Comparison of the SnowHydro snow sampler with existing snow tube designs. Hydrologic. Processes, 20, 2555-2562, DOI: 10.1002/hyp.9317, 2012.

Dong, C.: Remote sensing, hydrological modeling and in situ observations in snow cover research: A review. J. Hydrol., 561 (2018) 573–583, 2018.

Ducharme, P., Houdayer, A., Choquette, Y., Kapfer, B., and Martin, J. P.: Numerical Simulation of Terrestrial Radiation over A Snow Cover. J. Atmos. Ocean. Technol., 32, 1478-1485, 2015. (**GMON**)

Ellerbruch, D., and Boyne, H.: Snow Stratigraphy and Water Equivalence Measured with an Active Microwave System. J. Glaciol. 26, 225–233, 1980. (**FMCW-Radar**)

Fujino, K., Wakahama, G., Suzuki, M., Matsumoto, T., and Kuroiwa, D.: Snow stratigraphy measured by an active microwave sensor. Ann. Glaciol., 6, 207–210, 1985. (**FMCW-Radar**)

Goodison, B.E., Glynn, J.E., Harvey, K.D., and Slater, J.E.: Snow Surveying in Canada: A Perspective, Can. Water Resour. J., 12:2, 27-42, DOI: 10.4296/ cwrj1202027, 1987.

Goodison, B., Ferguson, H., and McKay, G.: Measurement and data analysis, in Handbook of Snow: Principles, Processes, Management and Use, pp. 191–274, Pergamon Press Canada, Toronto, Canada, 1981.

Gottardi, F., Carrier, P., Paquet, E., Laval, M.-T., Gailhard, J., and Garçon, R.: Le NRC: Une décennie de mesures de l'équivalent en eau du manteau neigeux dans les massifs montagneux français. In Proceedings of the International Snow Science Workshop Grenoble, 7–11 October 2013, 926–930, 1981. (**CNRP**)

GPRI brochure: GAMMA Portable Radar Interferometer (GPRI) https://gamma-rs.ch/uploads/media/Instruments_Info/gpri2_brochure_20160708.pdf , 2021. (**Radar**)

Gunn, G.E., Duguay, C.R., Brown, L.C., King, J., Atwood, D., and Kasurak, A.: Freshwater Lake Ice Thickness Derived Using Surface-based X- and Ku-band FMCW Scatterometers. Cold Reg. Sci. Technol., 120, 115–126, 2015. (**FMCW-Radar**)

Henkel, P., Koch, F., Appel, F., Bach, H., Prasch, M., Schmid, L., Schweizer, J., and Mauser, W.: Snow water equivalent of dry snow derived from GNSS Carrier Phases. IEEE Trans. Geosci. Remote Sens., 56(6), 3561–3572. https://doi.org/10.1109/TGRS.2018.2802494, 2018. (**GNSSR**)

Hu, X., Ma, C., Hu, R., and Yeo, T. S.: Imaging for Small UAV-Borne FMCW SAR. Sensors, 19, 87, doi: 10.3390/s19010087, 2019. (**FMCW-Radar**)

IMST: IMST sentireTM Radar Module 24 GHz sR-1200 Series User Manual. Available online: http://www.radar-sensor.com/, 2021 (**FMCW-Radar**)

Key, J., Goodison, B., Schöner, W., Godøy, Ø., Ondráš, M., and Snorrason, Á.: A Global Cryosphere Watch. Arctic, 68, 1, 48 – 58 . http://dx.doi.org/10.14430/arctic4476, 2015.

Kinar, N. J., and Pomeroy, J. W.: Measurement of the physical properties of the snowpack. Rev. Geophys. 53, 481–544. doi: 10.1002/2015RG000481, 2015.

King J., Kelly, R., Kasurak, A., Duguay, C., Gunn, G., Rutter, N., Watts, T., and Derksen C.: Spatio-temporal influence of tundra snow properties on Ku-band (17.2 GHz) backscatter. J. Glaciol., 61(226), doi: 10.3189/2015JoG14J020, 2015. (**Radar**)

Kirkham, J.D., Koch, I., Saloranta, T.M., Litt, M., Stigter, E.E., Møen, K., Thapa, A., Melvold, K., and Immerzeel, W.W.: Near Real-Time Measurement of Snow Water Equivalent in the Nepal Himalayas. Front. Earth Sci. 7:177. doi: 10.3389/feart.2019.00177, 2019. (**GMON**)

Koch, F., Henkel, P., Appel, F., Schmid, L., Bach, H., Lamm, M., Prasch, M., Jürg Schweizer, J., and Mauser, W.: Retrieval of snow water equivalent, liquid water content, and snow height of dry and wet snow by combining GPS signal attenuation and time delay. Water Resour. Res., 55, 4465–4487. https://doi.org/10.1029/ 2018WR024431, 2019. (**GNSSR**)

Koh, G., Yankielun, N.E., and Baptista, A.I.: Snow cover characterization using multiband FMCW radars. Hydrol. Process., 10, 1609–1617, 1996. (**FMCW-Radar**)

Laliberté, J., Langlois ,A., Royer, A., Madore, J.-B., and Gauthier, F.: Retrieving high contrasted interfaces in dry snow using a frequency modulated continuous wave (FMCW) Ka-band radar: a context for dry snow stability, Physical Geography, In revision (TPHY-S-21-00044), 2021. (**FMCW-Radar**) To be updated

Langlois, A.: Applications of the PR Series Radiometers for Cryospheric and Soil Moisture Research. Publisher: Radiometrics Corporation http://radiometrics.com/products-services/total_profiling/pr-series/, 2015. (**Radiometer**)

Larson, K., Gutmann, E., Zavorotny, V., Braun, J., Williams, M., and Nievinski, F.: Can we measure snow depth with GPS receivers? Geophys. Res. Lett., 36, L17502. https://doi.org/10.1029/2009GL039430, 2009. (**GNSSR**)

Larson, K. M., and Small, E. E.: Normalized microwave reflection index: A vegetation measurement derived from GPS networks, IEEE J. Sel. Topics Appl. Earth Observ. Remote Sens., 7(5), 1501-1511, doi: 10.1109/JSTARS.2014.2300116, 2014. (**GNSSR**)

Larson, K. M.: GPS interferometric reflectometry: Applications to surface soil moisture, snow depth, and vegetation water content in the western United States. Wiley Interdisciplinary Reviews: Water, 3(6), 775–787. https://doi.org/10.1002/wat2.1167, 2016. (**GNSSR**)

Larue, F., Royer, A., De Sève, D., Roy, A., Picard, G., Vionnet, V.: Simulation and assimilation of passive microwave data using a snowpack model coupled to a calibrated radiative transfer model over North-Eastern Canada, Water Resour. Res., 54, 4823–4848, https://doi. org/10.1029/2017WR022132, 2018.

Leinss, S., Wiesmann, A., Lemmetyinen, J., and Hajnsek, I.: Snow Water Equivalent of Dry Snow Measured by Differential Interferometry. IEEE J. Sel. Topics Appl. Earth Observ. Remote Sens., 8(8), 3773-379, 2015. (**SnowScat**)

Lejeune, Y., Dumont, M., Panel, J.-M., Lafaysse, M., Lapalus, P., Le Gac, E., Lesaffre, B., and Morin, S.: 57 years (1960–2017) of snow and meteorological observations from a mid-altitude mountain site (Col de Porte, France, 1325 m of altitude), Earth Syst. Sci. Data, 11, 71–88, https://doi.org/10.5194/essd-11-71-2019, 2019.

Marshall, H., Koh, G., and Forster, R.: Estimating alpine snowpack properties using FMCW radar. Ann. Glaciol., 40, 157–162, 2005. (**FMCW-Radar**)

Marshall, H.-P., Schneebeli, M., and Koh, G. Snow stratigraphy measurements with high-frequency FMCW radar: Comparison with snow micro-penetrometer. Cold Reg. Sci. Technol., 47, 108–117, 2007. (**FMCW-Radar**)

Marshall, H.-P., and Koh, G.: FMCW radars for snow research. Cold Reg. Sci. Technol., 52, 118–131, 2008.

Mätzler, C.: Microwave permittivity of dry snow, IEEE Trans. Geosci. Remote Sens., 48, 50–58, 1986.

Meloche, J., Langlois, A., Rutter, N., Royer, A., King, J., and Walker, B.: Characterizing Tundra snow sub-pixel variability to improve brightness temperature estimation in satellite SWE retrievals, The Cryosphere Discussion (Submitted tc-2021-156), 2021. To be updated

Meredith, M., Sommerkorn, M., Cassotta, S., Derksen, C., Ekaykin, A., Hollowed, A., Kofinas, G., Mackintosh, A., Melbourne-Thomas, J., Muelbert, M.M.C., Ottersen, G., Pritchard, H., Schuur, E.A.G.: Polar Regions. In: IPCC Special Report on the Ocean and Cryosphere in a Changing Climate [H.-O. Pörtner, D.C. Roberts, V. Masson-Delmotte, P. Zhai, M. Tignor, E. Poloczanska, K. Mintenbeck, A. Alegría, M. Nicolai, A. Okem, J. Petzold, B. Rama, N.M. Weyer (eds.)]. https://www.ipcc.ch/srocc/chapter/chapter-3-2/, 2019.

Murray, R. M., and Holbert, K. E.: Nuclear Energy: An Introduction to the Concepts, Systems, and Applications of Nuclear Processes, Eighth Edition, Imprint Butterworth-Heinemann, Elsevier Inc., 624 p. DOI https://doi.org/10.1016/C2016-0-04041-X, 2020. (**CNRP**)

Okorn, R., Brunnhofer, G., Platzer, T., Heilig, A., Schmid, L., Mitterer, C., Schweizer, J., and Eisen, O.: Upward-looking L-band FMCW radar for snow cover monitoring. Cold Reg. Sci. Technol., 103, 31–40, 2014. (**FMCW-Radar**)

Paquet, E. and Laval, M.T.: Retour d'expérience et perspectives d'exploitation des Nivomètres à Rayonnement Cosmique d'EDF / Operation feedback and prospects of EDF Cosmic-Ray Snow Sensors. La Houille Blanche 2006-2, 113-119, 2006. (**CNRP**)

Paquet, E., Laval, M., Basalaev, L. M., Belov, A., Eroshenko, E., Kartyshov, V., Struminsky, A., and Yanke, V.: An application of cosmic-ray neutron measurements to the determination of the snow-water equivalent, Proc. 30th Int. Cosm. Ray Conf., Mexico City, Mexico, 2008, 1, 761– 764, 2008. (**CNRP**)

Peng, Z., and Li, C.: Portable Microwave Radar Systems for Short-Range Localization and Life Tracking: A Review, Sensors, 19, 1136, 2019. (**FMCW-Radar**)

Pieraccini, M., and Miccinesi, L.: Ground-Based Radar Interferometry: A Bibliographic Review, Remote Sens., 11(9), 1029, 2019. https://doi.org/10.3390/rs11091029. (**Radar**)

Pirazzini, R., Leppänen, L., Picard, G., Lopez-Moreno, J. I., Marty, C., Macelloni, G., Kontu, A., von Lerber, A., Tanis, C. M., Schneebeli, M., de Rosnay, P., and Arslan, A. N.: European in-situ snow measurements: practices and purposes, Sensors 18:2016. doi: 10.3390/s18072016, 2018.

Prince, M., Roy, A., Royer, A., and Langlois, A.: Timing and Spatial Variability of Fall Soil Freezing in Boreal Forest and its Effect on SMAP L-band Radiometer Measurements, Remote Sens. Environ., 231, 111230, 2019.

Proksch, M., Rutter, N., Fierz, C., and Schneebeli, M.: Intercomparison of snow density measurements: Bias, precision, and vertical resolution, Cryosphere, 10, 371–384, 2016.

Rasmussen, R., Baker, B., Kochendorfer, J., Meyers, T., Landolt, S., Fischer, A. P., Black, J., Thériault, J. M., Kucera, P., Gochis, D., Smith, C., Nitu, R., Hall, M., Ikeda, K., and Gutmann, E.: How Well Are We Measuring Snow: The NOAA/FAA/NCAR Winter Precipitation Test Bed, Bull. Am. Meteorol. Soc., 93, 811–829, 2012.

Rodriguez-Morales, F., Gogineni, S., Leuschen, C.J., Paden, J.D., Li, J., Lewis, C. C., Panzer, B., Alvestegui, D. G-G., Patel, A., Byers, K., Crowe, R., Player, K., Hale, R., Arnold, E., Smith, L., Gifford, C., Braaten, D., and Panton, C.: Advanced multifrequency radar instrumentation for polar research. IEEE Trans. Geosci. Remote Sens. 52, 2824–2842, 2014. (**FMCW-Radar**)

Roy, A., Royer, A., St-Jean-Rondeau, O., Montpetit, B., Picard, G., Mavrovic, A., Marchand, N., and Langlois, A.: Microwave snow emission modeling uncertainties in boreal and subarctic environments, Cryosphere, 10, 623-638, http://www.the-cryosphere.net/10/623/2016/ doi:10.5194/tc-10-623-2016, 2016. (**Radiometer**)

Roy, A., Toose, P., Williamson, M., Rowlandson, T., Derksen, C., Royer, A., Berg, A., Lemmetyinen, J., and Arnold, L.: Response of L-Band brightness temperatures to freeze/thaw and snow dynamics in a prairie environment from ground-based radiometer measurements, Remote Sens. Environ., 191, 67-80, 2017. (**Radiometer**)

Rutter, N., Sandells, M., Derksen, C., Toose, P., Royer, A., Montpetit, B., Lemmetyinen, J., and Pulliainen, J.: Snow stratigraphic heterogeneity within ground-based pas- sive microwave radiometer footprints: implications for emis- sion modeling, J. Geophys. Res.-Earth Surf., 199, 550–565, https://doi.org/10.1002/2013JF003017, 2014.

Schattan, P., Baroni, G., Oswald, S. E., Schöber, J., Fey, C., Kormann, C., Huttenlau, M., and Achleitner, S.: Continuous monitoring of snowpack dynamics in alpine terrain by aboveground neutron sensing, Water Resour. Res., 53, 3615–3634, doi: 10.1002/2016WR020234, 2017. (**CNRP**)

Schneider, M.: Automotive radar—Status and trends. In Proceedings of the German Microwave Conference, Ulm, Germany, 5–7 April 2005; pp. 144–147, 2005. (**FMCW-Radar**)

Shah, R., Xiaolan Xu, Yueh, S., Sik Chae, C., Elder, K., Starr, B., and Kim, Y.: Remote Sensing of Snow Water Equivalent Using P-Band Coherent Reflection, IEEE Geosci. Remote Sens. Lett., 14, 3, 309-313, doi: ~~10.1109/LGRS.2016. 2636664~~, 2017. (**GNSSR**)

Sigouin, M. J. P., and Si, B. C.: Calibration of a non-invasive cosmic-ray probe for wide area snow water equivalent measurement. Cryosphere, 10, 1181–1190, 2016 www.the-cryosphere.net/10/1181/2016/, 2016. (**CNRP**)

Smith, C. D., Kontu, A., Laffin, R., and Pomeroy, J. W.: An assessment of two automated snow water equivalent instruments during the WMO solid precipitation intercomparison experiment, Cryosphere, 11, 101–116. doi: 10.5194/tc-11-101-2017, 2017. (**GMON**)

Stranden, H. B., Ree, B. L., and Møen, K. M.: Recommendations for Automatic Measurements of Snow Water Equivalent in NVE. Report of the Norwegian Water Resources and Energy Directorate, Majorstua, Oslo, Noway, 34 p., 2015. (**GMON**)

Tiuri, M., Sihvola, A., Nyfors, E., and Hallikainen, M.: The complex dielectric constant of snow at microwave frequencies. IEEE J. Ocean. Eng., 9, 377–382, 1984.

Vriend, N.M., McElwaine, J.N., Sovilla, B., Keylock, C.J., Ash, M., and Brennan, P. V.: High-resolution radar measurements of snow avalanches, Geophys. Res. Lett., 40, 727–731, 2013. (**FMCW-Radar**)

Werner, C., Wiesmann, A., Strozzi, T., Schneebeli, M., and Mätzler, C.: The SnowScat ground-based polarimetric scatterometer: Calibration and initial measurements from Davos Switzerland, in Proc. IEEE Int. Geosci. Remote Sens. Symp. (IGARSS'10), Jul. 2010, 2363–2366, 2010. (**SnowScat**)

Werner, C., Suess, M., Wegmüller, U., Frey, O., and Wiesmann A.: The Esa Wideband Microwave Scatterometer (Wbscat): Design and Implementation, in Proc. IGARSS 2019 - IEEE International Geoscience and Remote Sensing Symposium, 8339-8342, doi: 10.1109/IGARSS.2019.8900459, 2019. (**SnowScat**)

Wiesmann, A., Werner, C., Strozzi, T., Matzler, C., Nagler, T., Rott, H., Schneebeli, M., and Wegmüller, U.: SnowScat, X- to Ku-Band Scatterometer Development, in Proc. of ESA Living Planet Symposium, Bergen 28.6. - 2.7. https://gamma-rs.ch/uploads/media/Instruments_Info/gamma_snowscat.pdf, 2010. (**SnowScat**)

Wiesmann, A., Werner, C., Wegmüller, U., Schwank, M., and Mätzler, M.: ELBARA II, L-band Radiometer for SMOS Cal/Val Purposes, https://gamma-rs.ch/uploads/media/Instruments_Info/ELBARAII_poster.pdf, 2021. (**Radiometer**)

Wigneron, J.P., Jackson, T.J., O'Neill, P., De Lannoy, G.J., de Rosnay, P., Walker, J.P., Ferrazzoli, P., Mironov, V., Bircher, S., Grant, J.P., Kurum, M., Schwank, M., Munoz-Sabater, J., Das, N., Royer, A., Al-Yaari, A., Bitar, A. Fernandez-Moran, R., Lawrence, H., Mialon, A., Parrens, M., Richaume, P., Delwart, S., and Kerr Y.: Modelling the passive microwave signature from land surfaces: A review of recent results and application to the L-Band SMOS & SMAP soil moisture retrieval algorithms, Remote Sens. Environ., 192, 238–262, 2017. (**Radiometer**)

WMO: Global Cryosphere Watch (GCW) Implementation Plan, Version 1.6, World Meteorological Organization Report, WMO, Geneva, Switzerland, 2015.

Work, R. A., Stockwell, H. J., Freeman, T. G., and Beaumont, R. T.: Accuracy of field snow surveys, western United States, including Alaska, Cold Regions Research and Engineering Laboratory (U.S.) Technical report, 163, 49 p., https://hdl.handle.net/11681/5580. 1965.

Wright, M., Kavanaugh, K., and Labine C.: Performance Analysis of the GMON3 Snow Water Equivalency Sensor. Proceedings of The Western Snow Conference. Stateline, NV, USA, April 2011. Poster on line, https://www.campbellsci.ca/cs725, 2011 (**GMON**)

Wright, M.: CS725 Frozen Potential: The Ability to Predict Snow Water Equivalent is Essential. METEOROLOGICAL TEChnOLOGy InTERnATIOnAL, August 2013, 122-123, https://www.meteorologicaltechnologyinternational.com, 2013. (**GMON**)

Xu, X., Baldi, C., Bleser, J.-W., Lei, Y., Yueh, S., and Esteban-Fernandez, D.: Multi-Frequency Tomography Radar Observations of Snow Stratigraphy at Fraser During SnowEx, in Proceedings of the IGARSS 2018-2018 IEEE International Geoscience and Remote Sensing Symposium, Valencia, Spain, 22–27 July 2018, 2018. (**FMCW-Radar**)

Yankielun, N.E., Ferrick, M.G., and Weyrick, P. B.: Development of an airborne millimeter-wave FM-CW radar for mapping river ice, Can. J. Civ. Eng., 20, 1057–1064, 1993. (**FMCW-Radar**)

Yankielun, N., Rosenthal, W., and Robert, D.: Alpine snow depth measurements from aerial FMCW radar. Cold Reg. Sci. Technol., 40, 123–134, 2004. (**FMCW-Radar**)

Yao, H., Field, T., McConnell, C., Beaton, A., and James A.L.: Comparison of five snow water equivalent estimation methods across categories. Hydrol. Process., 32, 1894–1908, https://doi.org/10.1002/hyp.13129, 2018. (**GMON**)